Soft Matter

PAPER

View Article Online
View Journal | View Issue

Cite this: *Soft Matter*, 2026, **22**, 1141

Predicting bio-corona-induced adsorption and uptake of nanoplastics

Wenlin Zhang * and Anderson D. S. Duraes

Received 23rd November 2025,
Accepted 11th January 2026

DOI: 10.1039/d5sm01170a

rsc.li/soft-matter-journal

We employ a theoretical approach to predict bio-corona-induced uptake of nanoplastics (NPLs) across plasma membranes (PMs). A lattice self-consistent field theory (SCFT) is used to model the formation of bio-coronae, which are composed of biopolymers adsorbed on NPLs. As the NPL approaches the PM, we show that weak monomer–PM attractions allow the adsorbed biopolymers to redistribute between the two surfaces. This rearrangement can reduce crowding in the bio-corona and induce an effective attraction between the NPL and the membrane. Using the theory of elasticity for lipid membranes, we show that a weak effective attraction enables NPLs to bind to cell membranes, generating excess stress and increasing elastic free energy in the biological barrier. When the effective NPL–PM interactions are sufficiently strong, nanoplastics can be spontaneously internalized by cells within a short time.

1 Introduction

Microplastics (MPLs) and nanoplastics (NPLs) are either intentionally manufactured small plastic particles[1] or formed from discarded plastics through chemical and mechanical degradation.[2] These small particles may enter the human body *via* ingestion, inhalation, or skin contact, posing potential health risks.[3–5] For instance, a recent study indicates that exposure to MPLs and NPLs may increase the risk of cardiovascular diseases.[6] However, the interactions of MPLs and NPLs with biological systems at the molecular level remain poorly understood. To develop a mechanistic understanding of the fate of NPLs in the human body and assess their potential health impacts, quantifying the interactions between MPLs/NPLs and plasma membranes (PMs), which serve as barriers that prevent small plastic particles from entering cells, is essential.[7]

Experimentally characterizing the interactions between MPLs/NPLs and plasma membranes is challenging. Most previous experimental studies demonstrating the cellular uptake of these particles have relied on model colloidal polystyrene (PS) spheres with surface charges.[8] Yet, model PS particles may not capture the wide range of physicochemical properties exhibited by MPLs and NPLs, such as semicrystallinity and hydrophobicity, that may influence particle–membrane interactions. Moreover, characterizing the molecular interactions of MPLs and NPLs with PMs, particularly for small nanoparticles, remains challenging.[9,10] Extrapolating results obtained from model colloidal PS particles to smaller NPLs with different molecular structures requires further validation.

Department of Chemistry, Dartmouth College, Hanover, New Hampshire 03755, USA. E-mail: wenlin.zhang@dartmouth.edu

The spatiotemporal resolutions of atomistic simulations can provide valuable insights into the NPL–PM interactions. Although such simulations can accurately describe the physicochemical properties of MPLs, NPLs, and PMs, they remain limited in accessible length and time scales.[11] Thus, atomistic simulations are only feasible for investigating small NPLs (with diameters on the order of nanometers) in the vicinity of PMs.

To model larger particles, coarse-grained (CG) approaches are required. Popular CG molecular dynamics models, such as the MARTINI,[12–14] however, do not always reproduce the physicochemical properties of MPLs and NPLs accurately. Misrepresentations of NPLs/MPLs properties, such as the absence of crystalline order, can introduce artifacts in the effective interactions between plastic particles and PMs.[15]

Existing CG simulation models also employ resolutions that are not coarse enough to simulate large-scale phenomena, which could be critical for NPLs uptake. In our previous work, we showed that passive diffusion of bare NPLs across lipid membranes requires local bilayer fracture, leading to a high free energy barrier even for the cellular uptake of small NPLs (3–5 nm in size).[15] If NPLs exhibit sufficiently strong attraction to PMs, they can adsorb onto the lipid surface, become wrapped by the membrane, and eventually be pinched off into the cell. Such a budding process of adsorbed particles represents a viable cellular uptake mechanism for colloidal particles, including the nucleocapsids of animal viruses.[16] Still, this passive uptake pathway remains difficult to simulate using conventional CG approaches.

In this work, we apply a theoretical approach to predict the effective attraction between a nanoplastic and a plasma membrane, induced by biomacromolecules adsorbed on the NPL surface. Indeed, the adsorption of NPLs of commodity

plastics could depend on the degree and type of degradation, which may strongly modify the surface chemistry of the particles. Still, bare particles of commodity polymer, such as polyethylene (PE), do not adhere to lipid membranes.[15] Nonetheless, organic species, such as humic and fulvic acids, and biopolymers, including proteins and alginate, can adsorb onto NPL surfaces to form the so-called "eco-corona" or "bio-corona".[17,18] This adsorbed layer of organic molecules can induce effective attraction between NPLs and PMs. Together with the theory of elasticity for lipid membranes, we use the theoretical model to show how the bio-corona-induced interactions impact the adsorption of NPLs onto PMs and facilitate their subsequent cellular uptake.

Our paper is organized as follows. (1) In the Methods section, we first introduce a lattice version of self-consistent field theory (SCFT) to describe the adsorption of biopolymers onto NPL surfaces and the formation of the bio-corona. (2) Based on the predicted density profile of the bio-corona, we show how to estimate the effective attraction between an NPL and a lipid membrane. In our model, we consider polymers to experience short-ranged attraction towards the NPL and PM surfaces and exhibit excluded volume interactions in solutions and adsorbed layers. (3) We then describe a theoretical approach, combining the predicted attraction with the elastic free energy of lipid membranes, to estimate NPL adsorption and passive uptake. Readers less interested in the technical details of our approach could refer directly to the Results section. (4) In the Results section, we apply our approach to demonstrate how the molecular properties of polymer layers affect the adsorption and uptake of NPLs in a model NPL–PM system. (5) Finally, in the Discussion section, we outline how our theoretical model can be integrated with atomistic simulations to predict the effects of realistic biomacromolecules on NPL adsorption and uptake.

2 Methods

2.1 Predicting biopolymer adsorption and bio-corona formation

We employ a lattice-based self-consistent field theory (SCFT) to estimate the adsorption of biopolymers, such as intrinsically disordered proteins and polypeptides, onto NPLs. Similar approaches have been used to investigate the self-assembly of block copolymers[19–21] and adsorption of telechelic polymers onto colloidal particles.[22]

Considering the biopolymers near the NPLs to be in the marginal regime, the interactions between polymer segments are governed by pairwise, excluded-volume interactions:[23]

$$\beta F_{\text{int}} = \frac{1}{2} v \int c(\mathbf{r})^2 \mathrm{d}^3\mathbf{r}, \tag{1}$$

where $\beta = 1/kT$, v is the excluded volume (which enforces that two segments cannot occupy the same space), and $c(\mathbf{r})$ is the local concentration of polymer (Kuhn) segments of length b. In the marginal regime, satisfied when $v/b^3 \ll 1$, a polymer chain behaves as a random walk of N Kuhn segments of length b at all length scales.

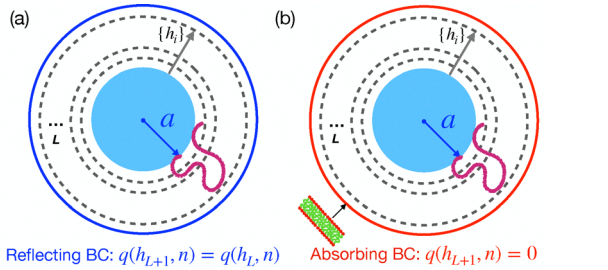

Fig. 1 (a) Discretized lattice used to calculate adsorbed biopolymers around a spherical NPL of radius a. (b) Discretized lattice for adsorbed biopolymers confined between NPL and PM (red) surfaces.

We compute the distribution of biopolymers near an NPL of radius a by discretizing the space around the particle into a pseudo-one-dimensional lattice $\{h_i\}$ with lattice spacing b (Fig. 1a), such that the radial distance from the particle surface is $\Delta H = h_i b$. A local chemical potential field $W(h_i)$ biases the polymer random walks and is governed by the excluded-volume interactions between Kuhn monomers and a short-ranged surface attraction ε:

$$\beta W(h_i) = v c(h_i) + \varepsilon(h_i) \tag{2}$$

in which the short-ranged attraction ε acts only on monomers located in the surface layer adjacent to the NPL:

$$\varepsilon(h_i) = \begin{cases} \delta_1 & \text{if } h_i = h_1 \text{ (surface layer next to NPL)} \\ 0 & \text{if } h_i \neq h_1 \end{cases} \tag{3}$$

where δ_1 quantifies the weak attraction between a monomer and the NPL surface.

The conditional Boltzmann weight (propagator) for placing the first monomer in a lattice layer is

$$q(h_i,1) = \mathrm{e}^{-\beta W(h_i)} \tag{4}$$

which evolves according to a recursion relation, discretized as:

$$\begin{aligned} q(h_i, n) \; = \{ & \lambda_- q(h_{i-1}, n-1) + \lambda_0 q(h_i, n-1) \\ & + \lambda_+ q(h_{i+1}, n-1) \} \mathrm{e}^{-\beta W(h_i)} \end{aligned} \tag{5}$$

The transition probabilities λ_-, λ_0, and λ_+ correspond to the displacement of the nth Kuhn segment from monomer $n-1$ to layer i, originating from layers $i-1$, i, and $i+1$, respectively.[21]

When the size of the NPLs is much larger than that of the polymer, the surface can be approximated as a flat wall. In this case, λ_-, λ_0, and λ_+ take the values 1/6, 4/6 and 1/6, respectively, reflecting the fractions of nearest neighbors on the cubic lattice in each of the three layers where the next Kuhn step may reside. For polymers whose sizes are comparable to that of the NPL, we place them on a spherical lattice. In this case, the transition probabilities λ_-, λ_0, and λ_+ depend on the radial distance from the particle center and are given by: $(a + h_i - b)/(6(a + h_i))$, 4/6, and $(a + h_i + b)/(6(a + h_i))$, respectively. This variation arises because the number of sites differs across lattice layers.

To evolve the propagators, we impose a non-penetration boundary adjacent to the NPL and a reflecting boundary at the outer lattice, such that

$$q(h_0, n) = 0 \quad \text{and} \quad q(h_{L+1}, n) = q(h_L, n), \tag{6}$$

where L denotes the number of lattice layers.

The Boltzmann weight for the nth chain segment to occupy the ith layer is

$$Q(h_i, n) = q(h_i, n)q(h_i, N - n + 1)e^{\beta W(h_i)} \tag{7}$$

We use the exponential term in eqn (7) to cancel the double-counting of the local chemical potential $e^{-\beta W(h_i)}$ in the two propagators for placing the nth monomer at h_i. The single-chain partition function Z is thus the sum of Boltzmann weights for all chain configurations in which the nth monomer occupies any lattice layer:

$$Z = \sum_{i=1}^{L} A(h_i)Q(h_i, n) \tag{8}$$

where $A(h_i)$ is the number of sites in the ith lattice layer. On a spherical lattice, $A(h_i) = 4\pi(a + h_i)^2$, whereas on a cubic lattice, $A(h_i)$ is constant for all h_i. The density distribution $c(h_i)$ is then calculated as:

$$c(h_i) = \frac{C}{Z}\sum_{n=1}^{N} Q(h_i, n), \tag{9}$$

where C is chosen such that $c(h_L) = c_0$, which represents the bulk concentration of the biopolymers. The concentration distribution $c(h_i)$ is iteratively updated, as it determines the local chemical potential field $W(h_i)$, until self-consistency is achieved—that is, when the input and output concentration distributions are identical.

The local concentration profile includes contributions from both adsorbed chains and free polymers. To characterize the bio-corona, we compute the Boltzmann weight distribution $Q_{\text{ads}}(h_i, n)$ for the adsorbed chains, defined as those for which at least one monomer resides in the first lattice layer adjacent to the NPL. To this end, we evolve the propagator $q_{\text{free}}(h_i, n)$ of free chains in the known chemical potential field $W(h_i)$ after obtaining the self-consistent concentration profile $c(h_i)$. The first lattice layer h_1 is then treated as an absorbing boundary, while the reflecting boundary is retained at the outer lattice:

$$q_{\text{free}}(h_1, n) = 0 \quad \text{and} \quad q_{\text{free}}(h_{L+1}, n) = q_{\text{free}}(h_L, n). \tag{10}$$

The initial condition for the free chain propagator is

$$q_{\text{free}}(h_i, 1) = e^{-\beta W(h_i)} \quad (i > 1), \tag{11}$$

and the Boltzmann weight for placing the nth segment of a free chain at h_i is given by

$$Q_{\text{free}}(h_i, n) = q_{\text{free}}(h_i, n)q_{\text{free}}(h_i, N - n + 1)e^{\beta W(h_i)}. \tag{12}$$

With this, the Boltzmann weight for the adsorbed chains is $Q_{\text{ads}}(h_i, n) = Q(h_i, n) - Q_{\text{free}}(h_i, n)$, while the concentration profile of the free chains is:

$$c_{\text{free}}(h_i) = \frac{CA(h_i)}{Z}\sum_{n=1}^{N} Q_{\text{free}}(h_i, n), \tag{13}$$

where C again ensures that $c_{\text{free}} = c_0$ at large L. The concentration profile of the adsorbed chains is then given by:

$$c^0_{\text{ads}}(h_i) = c(h_i) - c_{\text{free}}(h_i) \tag{14}$$

2.2 Estimating bio-corona-induced NPL–PM attraction

We assume that free chains are washed away when NPLs are transported in biological systems, leaving the adsorbed chains to form the bio-corona. As we demonstrate in the Results section (Section 3), peeling off an adsorbed chain is relatively difficult. To obtain the shape of the unperturbed bio-corona concentration c_{ads}, we remove the free chains near the NPL and re-equilibrate the adsorbed chains with a total number of monomers:

$$J = \sum_{i=1}^{L} A(h_i)c^0_{\text{ads}}(h_i) \tag{15}$$

We compute the conditional Boltzmann weight $Q_{\text{ads}}(h_i, n)$ for the adsorbed chains, from which the new partition function and concentration profile of the bio-corona are:

$$Z_{\text{ads}} = \sum_{i=1}^{L} A(h_i)Q_{\text{ads}}(h_i, n) \tag{16}$$

and

$$c_{\text{ads}}(h_i) = \frac{J}{NZ_{\text{ads}}}\sum_{n=1}^{N} Q_{\text{ads}}(h_i, n), \tag{17}$$

where J/N is the total number of chains.

After finding the self-consistent concentration field $c_{\text{ads}}(h_i)$, the free energy per chain for the unperturbed bio-corona is:

$$\beta F_{\text{ads}} = -\ln Z_{\text{ads}} - \frac{N}{2J}\sum_{i=1}^{L} A(h_i)v\{c_{\text{ads}}(h_i)\}^2 + \ln\frac{J}{N} \tag{18}$$

where the second term cancels the double-counted pairwise excluded-volume interactions, and the third term accounts for the indistinguishability of the adsorbed chains.

To estimate the effective NPL–PM attraction induced by the bio-corona, we consider an extreme scenario in which a PM is forced to fully wrap around an NPL (Fig. 1b). In this configuration, the bio-corona is confined between the surfaces of the NPL and PM. This confinement, together with a polymer–PM interaction, perturbs the concentration distribution and free energy of the biopolymers. To obtain the new concentration profile, we convert the outer lattice layer, representing the lipid membrane surface, from a reflecting boundary to an adsorbing boundary,

$$q_{\text{ads}}(h_{L+1}, n) = 0. \tag{19}$$

Thus, monomers in the Lth layer now experience a short-range attraction δ_2 from the PM:

$$\varepsilon(h_i) = \begin{cases} \delta_1 & \text{if } h_i = h_1 \text{ (surface layer next to NPL)} \\ \delta_2 & \text{if } h_i = h_L \text{ (surface layer next to PM)} \\ 0 & \text{if } h_i \neq h_1, h_L \end{cases} \quad (20)$$

which modifies $W(h_i)$ when the confinement is sufficient for the PM to contact the outer surface of the bio-corona.

We re-equilibrate the biopolymers between the two attractive yet impenetrable surfaces to obtain a new concentration profile and free energy of the bio-corona. This is achieved by evolving the propagator $q_{\text{ads}}(h_i, n)$ from the initial condition in eqn (4) *via* the recursion relation in eqn (5). From $q_{\text{ads}}(h_i, n)$, the new Boltzmann weight $Q_{\text{ads}}(h_i, n)$ (eqn (7)) can be computed, from which the new partition function (eqn (16)), concentration profile (eqn (17)), and free energy (eqn (18)) of the biopolymers confined between the NPL and PM are obtained. By varying the confinement L, we identify a minimum in $\Delta F^* = F_{\text{ads}} - F^0_{\text{ads}}$ at L^*, induced by the bio-corona, where F^0_{ads} is the free energy of a biopolymer chain in the unperturbed bio-corona. The attraction per unit area between the NPL and PM can then be estimated as

$$w = \frac{J\Delta F^*}{4\pi(a + bL^*)^2 N}. \quad (21)$$

2.3 Free energy of PM wrapping around an NPL

Nanoplastics (NPLs) generated from the degradation of commodity plastic products can exhibit various shapes. To simplify the problem, we model an NPL as a rigid spherical particle with radius a. The formation of a bio-corona makes the particle slightly bulkier, giving it an effective radius $a^* = a + bL^*$. Nonetheless, we expect that polymer-coated NPLs do not deform significantly upon contact with the lipid membrane. Therefore, the wrapping process can be treated under cylindrical symmetry,[24,25] and we divide the lipid membrane into two regions: an adhesion region, where the NPL interacts with the membrane, and an outer free region, where the membrane bends to accommodate the NPL-induced deformation in the adhesion region (Fig. 2).

To describe the adhesion region and quantify the degree of NPL wrapping, we introduce a contact angle α, which defines the point where the lipid membrane begins to detach from the surface of the spherical particle (see Fig. 2). By varying α, we control the degree of wrapping, expressed as

$$z = (1 - \cos\alpha)/2, \quad (22)$$

which ranges from zero (no wrapping) to unity (full wrapping).

The free energy of the wrapped region includes the stretching and bending contributions associated with deforming an initially flat membrane. Assuming the PM has an interfacial tension σ and that its relative area change is negligible, we estimate the stretching free energy cost from the excess area pulled toward the wrapping site, $\Delta A_{\text{ex}} = 4\pi a^{*2} z^2$, as:[24]

$$F_{\text{stretch}} = \Delta A_{\text{ex}}\sigma = 4\pi a^{*2} z^2 \sigma, \quad (23)$$

where ΔA_{ex} represents the difference between the NPL cap area covered by the PM and the projected area of the NPL (a disk) on the PM.[15]

The bending free energy cost is governed by the bending modulus κ and the NPL cap area covered by the PM (adhesion region) $A_{\text{ad}} = 4\pi a^{*2} z$:[15,24]

$$F_{\text{bend}} = \frac{1}{2}\kappa\left(\frac{2}{a^*}\right)^2 A_{\text{ad}} = 8\pi\kappa z \quad (24)$$

The interactions between the bio-corona and the PM contribute an adhesion energy F_{bio}:

$$F_{\text{bio}} = wA_{\text{ad}} = 4\pi w a^{*2} z \quad (25)$$

in which w is the adhesion energy per unit area of nanoparticle induced by the adsorbed bio-macromolecules. The total free energy of the adhesion region of the membrane is thus given by

$$F_1 = F_{\text{stretch}} + F_{\text{bend}} + F_{\text{bio}} \quad (26)$$

By introducing the dimensionless interfacial tension $\tilde{\sigma} = \sigma a^2/\kappa$ and the dimensionless adhesion strength $\tilde{w} = 2wa^2/\kappa$, the dimensionless free energy of the adhesion region can be written as

$$\tilde{F}_1 = \frac{F_1}{\pi\kappa} = 4\tilde{\sigma}z^2 + (8 + 2\tilde{w})z \quad (27)$$

To fully describe the free energy of NPL wrapping, we next solve for the shape profile and the associated elastic energy $\tilde{F}_2$ (normalized by $\pi\kappa$) of the outer region of the membrane (see Fig. 2). Following the approach of Deserno,[24] we write:

$$\tilde{F}_2 = \int_0^S \mathrm{d}s L\left(\psi, \dot{\psi}, r, \dot{r}, h, \dot{h}, \lambda_r, \lambda_h\right), \quad (28)$$

where the dot denotes a derivative with respect to the arclength s, $s = 0$ corresponds to the contact point of the outer membrane with the NPL, $s = S$ is a reference point far from the NPL–PM adsorption region, and the functional L is

$$L = r\left\{\left(\dot{\psi} + \frac{\sin\psi}{r}\right)^2 + 2\tilde{\sigma}(1 - \cos\psi)\right\} + \lambda_r(\dot{r} - \cos\psi) + \lambda_h(\dot{h} - \sin\psi) \quad (29)$$

The terms in the curly brackets in eqn (29) represent the bending (quadratic) and stretching free energy, while λ_r and λ_h

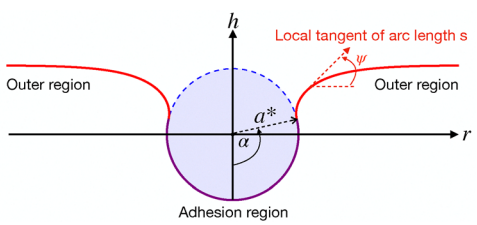

Fig. 2 Schematic of an NPL of radius a^* wrapped by an initially flat PM. The adhesion region (purple) is described by a contact angle α, while the outer stretched region (red) is modeled by the tangent angle ψ along the arclength s, measured with respect to the horizontal axis r.

are Lagrange multipliers enforcing the parametrization constraints of the outer membrane shape, as defined in Fig. 2. The term $\dot{x}$ denotes $\mathrm{d}x/\mathrm{d}s$, and the length parameters r, h, and s are normalized by $a^\star$.

Minimization of the elastic free energy functional $\tilde{F}_2$,[26]

$$\frac{\partial L}{\partial x} - \frac{\mathrm{d}}{\mathrm{d}s}\left(\frac{\partial L}{\partial \dot{x}}\right) = 0, \tag{30}$$

where $x = \psi, \dot{\psi}, r, \lambda_r, \lambda_h$, yields the following system of ordinary differential equations:

$$\dot{\psi} = \frac{p_\psi}{2r} - \frac{\sin\psi}{r}, \tag{31a}$$

$$\dot{r} = \cos\psi, \tag{31b}$$

$$\dot{h} = \sin\psi, \tag{31c}$$

$$\dot{p}_\psi = \frac{p_\psi}{r}\cos\psi + (2\tilde{\sigma}r + p_r)\sin\psi, \tag{31d}$$

$$\dot{p}_r = \frac{p_\psi}{r}\left(\frac{p_\psi}{4r} - \frac{\sin\psi}{r}\right) + 2\tilde{\sigma}(1-\cos\psi), \tag{31e}$$

where

$$p_\psi = \frac{\partial L}{\partial \dot{\psi}} = 2r\left(\dot{\psi} + \frac{\sin\psi}{r}\right), \tag{32a}$$

$$p_r = \frac{\partial L}{\partial \dot{r}} = \lambda_r. \tag{32b}$$

At $s = 0$, we impose three boundary conditions that can be identified from Fig. 2 and summarized in eqn (33). Far from the NPL and PM contact, $s = S \to \infty$, the membrane should remain unperturbed and asymptotically flat. By allowing the profile variables r and h to vary freely during minimization, Deserno[24] showed that this condition is satisfied by setting $\psi(S) = \dot{\psi}(S) = 0$, and by applying eqn (30) for $x = \dot{r}$ and $\dot{h}$ at S, which yield

$$\begin{cases} \psi(0) = \alpha \\ r(0) = \sin\alpha \\ h(0) = -\cos\alpha \\ p_\psi(S) = 0 \\ p_r(S) = 0 \end{cases} \tag{33}$$

Applying eqn (30) to the remaining variable $x = h$ and similarly for $x = \dot{h}$ at the boundary S (as above) implies $\lambda_h = 0$ everywhere.

The system in eqn (31), together with the boundary conditions in eqn (33), defines a boundary value problem that we solve using a collocation algorithm.[27] Alternatively, the system in eqn (31) can be solved by converting the boundary value problem into an equivalent initial value problem. Deserno[24] employed this approach with the following initial boundary conditions:

$$\begin{cases} \psi(0) = \alpha \\ r(0) = \sin\alpha \\ h(0) = -\cos\alpha \\ p_\psi(0) = 2r\left(\dot{\psi}(0) + \dfrac{\sin\alpha}{r}\right) \\ p_r(0) = \dfrac{2\sqrt{z(1-z)}}{1-2z}\left\{1 + 4\tilde{\sigma}z - \left[\dot{\psi}(0)\right]^2\right\} \end{cases} \tag{34}$$

In this approach, the initial boundary condition $\dot{\psi}(0)$ is unknown and must be iteratively adjusted so that $\psi(S) \to 0$ at a sufficiently large value of S, a procedure known as the shooting method.[27]

For a given $\tilde{\sigma}$ and contact angle α (or equivalently, wrapping degree z (eqn (22)), we numerically solve for the shape of the outer membrane region, obtaining ψ, r, h, p_ψ and p_r. The derivative $\dot{\psi}$ is then extracted from p_ψ using eqn (32a). With these shape functions, we compute $\tilde{F}_2$ in eqn (28) using Simpson's rule.[26]

Combining the elastic free energy of the outer region (eqn (28)) with the adhesion free energy (eqn (27)) yields the total dimensionless free energy,

$$\Delta\tilde{F} = \tilde{F}_1(\tilde{w}, \tilde{\sigma}, z) + \tilde{F}_2(\tilde{\sigma}, z). \tag{35}$$

Because $\tilde{F}_2$ is independent of $\tilde{w}$, it only needs to be computed once to obtain $\Delta\tilde{F}$ profiles for a fixed $\tilde{\sigma}$ and z while varying $\tilde{w}$. To highlight the elastic free energy of PM induced by NPL adsorption, we set $\tilde{w} = 0$ in eqn (35) and write

$$\Delta\tilde{F}_{\mathrm{el}} = \tilde{F}_1(0, \tilde{\sigma}, z) + \tilde{F}_2(\tilde{\sigma}, z). \tag{36}$$

3 Results

To demonstrate our computational framework, we consider biopolymers composed of N Kuhn segments of length b = 1 nm adsorbed onto an NPL of radius a = 50 nm. The bulk biopolymer concentration is $c_0 = 0.1b^{-3}$, and the excluded volume parameter is $v = 0.1b^3$. Using the lattice SCFT model, we compute the density distribution of polymer segments around the spherical NPL (Fig. 3a). For the rather large NPL here, we consider the polymer–NPL and polymer–PM interfaces to be flat. Large NPL radius only leads to a negligible difference (less than b/a) between the transition probabilities λ_+ and λ_- in a spherical lattice for curved interfaces and those in a cubic lattice for flat interfaces. As expected, adsorbed loops and tails accumulate near the NPL surface, depleting the free, non-adsorbed chains in the bio-corona. The adsorption layer becomes thicker with increasing chain length N (Fig. 3b), as longer chains can form more extended loops and tails around the particle. Increasing the polymer–NPL attraction δ_1 also produces a denser adsorption layer (Fig. 3c).

To obtain the shape of the unperturbed bio-corona, we remove the free chains near the NPL and re-equilibrate the adsorbed chains. The concentration profile of the bio-corona remains largely unchanged (Fig. 4a and b). In a marginal solution, the adsorbed polymer chains behave approximately as ideal random walks, neither swelling nor collapsing when additional solvent enters the corona to replace the free chains. Therefore, we assume the thickness of the bio-corona $L^\star$ is governed by the polymer molecular weight and scales as $L^\star \approx N^{1/2}$, the characteristic size of Gaussian chains.[28]

We can assess the stability of the bio-corona by "peeling off" an adsorbed polymer chain. Because the absorbed chains behave as ideal random walks at all length scales in the

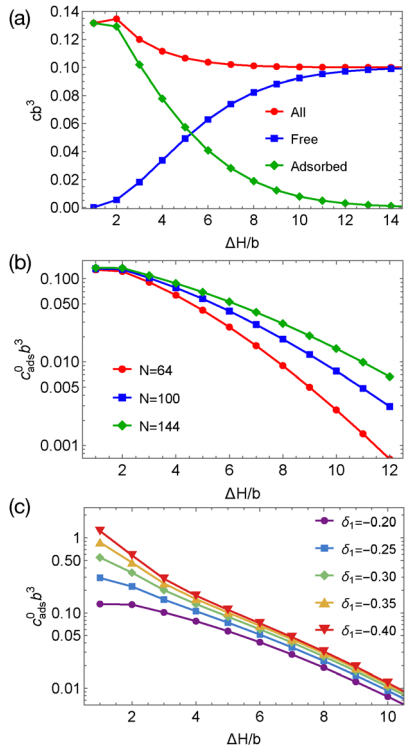

Fig. 3 (a) Concentration profiles of the total, adsorbed, and free biopolymers with N = 100 and excluded volume v = $0.1b^3$ around an NPL. Polymer–NPL attraction δ_1 = −0.2. (b) Adsorbed polymer concentration profiles for chains of different lengths at δ_1 = −0.2. (c) Adsorbed polymer concentration profiles for chains with N = 100 at various attraction strengths δ_1. Concentrations are plotted as a function of radial distance from the NPL surface. Bio-coronae formed in solutions with c_0 = $0.1b^{-3}$.

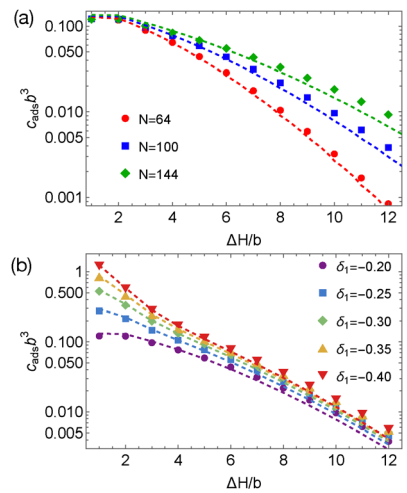

Fig. 4 (a) Concentration profiles of unperturbed bio-coronae for different adsorbed polymer chain lengths N. Polymer–NPL attraction δ_1 = −0.2. (b) Concentration profiles of unperturbed bio-coronae (N = 100) for different polymer–NPL attraction strengths δ_1. Concentration profiles of adsorbed polymers in the presence of free chains (dashed curves). Concentrations are plotted as a function of radial distance from the NPL surface. Bio-coronae formed in solutions with c_0 = $0.1b^{-3}$.

marginal regime, we assume the peeled chain adopts nearly the same configuration as the adsorbed molecules, except that none of its monomers are in contact with the NPL surface. This configuration corresponds to the maximum free energy of the detached chain, as its monomers no longer experience the attractive interaction with the NPL surface but still experience excluded volume interactions within the crowded bio-corona. Accordingly, we estimate the mean free energy barrier for detaching an adsorbed chain as

$$\beta\Delta F_{\text{detach}} \approx -\delta_1 4\pi a^2 c_{\text{ads}}(h_1) bN/J, \qquad (37)$$

where $c_{\text{ads}}(h_1)b$ represents the number of adsorbed monomers per unit area and J/N is the total number of chains. We assume that $c_{\text{ads}}(h_1)$ is approximately uniform across the layer h_1. The detachment free energy barrier increases with both polymer molecular weight and monomer–NPL attraction (Fig. 5). For sufficiently long adsorbed chains, $\beta\Delta F_{\text{detach}}$ can reach many kT, indicating that the adsorbed polymers remain stable even after the free chains are washed away.

To estimate the bio-corona-induced attraction between the NPL and PM, we allow the PM to fully wrap the polymer-coated NPL with a varying confinement parameter L (Fig. 1). For each value L between the NPL and PM, the distribution of polymer segments is re-equilibrated. A weak polymer–PM attraction δ_2 results in a more uniform polymer density around the NPL across different confinements (Fig. 6a).

Tuning the confinement L varies the interaction between the coated NPL and the PM. For sufficiently large L, the additional polymer–PM attraction allows polymer segments to redistribute and reduce their crowding near the NPL surface, which increases their translational entropy and lowers βF_{ads} (Fig. 6b). However, even with this added attraction, decreasing L increases confinement and forces the polymer segments into a more crowded state. This strengthens excluded volume interactions and reduces translational entropy, therefore increasing βF_{ads}. As a result, compressing the bio-corona generates repulsive forces between the NPL and PM. We thus assign an effective size $a^* = a + bN^{1/2}$ to a bio-corona-coated NPL. This effective size is then used to calculate the surface attraction w (eqn (21)) that drives NPL uptake.

We calculate the dimensionless surface attraction $\tilde{w}$ that drives the NPL adsorption and uptake using eqn (21) and the

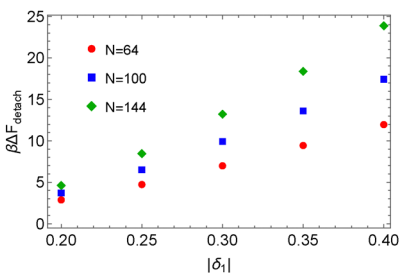

Fig. 5 Detachment free energy barrier for an adsorbed chain in a bio-corona $\beta\Delta F_{\text{detach}}$ *vs.* monomer–NPL attraction strength $|\delta_1|$ (eqn (37)). Bio-coronae formed in solutions with c_0 = $0.1b^{-3}$.

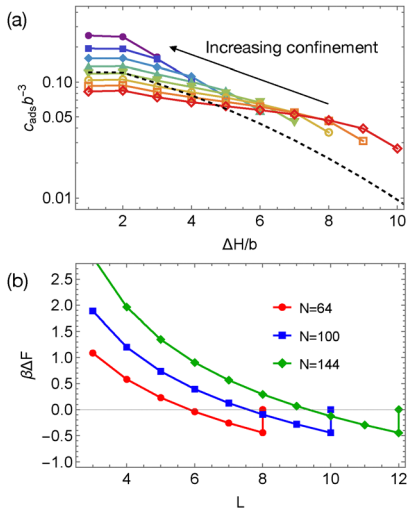

Fig. 6 (a) Concentration distributions in bio-corona (N = 100 and $\delta_1 = -0.2$) between an NPL wrapped by a PM with a polymer–PM attraction $\delta_2 = -0.15$. Unperturbed bio-corona (dashed) and concentration distributions as a function of radial distance with a varying confinement (colors). Purple corresponds to a system with the closest distance between NPL and PM surfaces. (b) Free energy change per adsorbed chain $\beta\Delta F = \beta F_{ads} - \beta F^0_{ads}$ *vs.* degree of confinement (in number of lattice layers L) for polymers of different lengths; $\delta_2 = -0.15$. Bio-coronae formed in solutions with $c_0 = 0.1b^{-3}$.

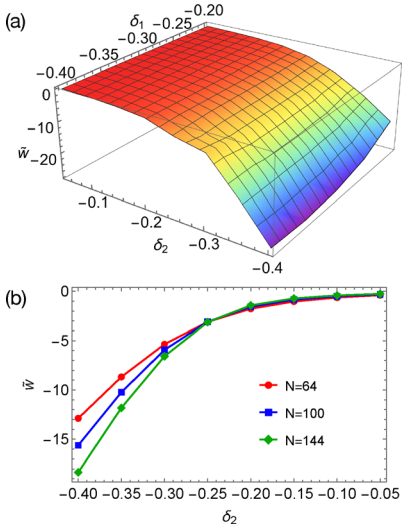

Fig. 7 (a) Effective interactions induced by bio-corona, consisting of polymers with N = 100, *vs.* polymer–NPL and polymer–PM interactions. (b) Chain length dependence of $\tilde{w}$ for fixed polymer–NPL attraction $\delta_1 = -0.2$ and various polymer–PM interactions δ_2. All bio-coronae formed in solutions with $c_0 = 0.1b^{-3}$.

conversion described in Section 2.3. The value of $\tilde{w}$ increases with the polymer–surface interaction strengths δ_1 and δ_2 (Fig. 7a). The polymer–NPL interaction δ_1 enhances the density of the bio-corona, and together with the polymer–PM attraction δ_2, a denser bio-corona leads to a stronger effective attraction between the NPL and PM. Longer chains also lead to a stronger effective attraction $\tilde{w}$ (Fig. 7b).

Using the predicted $\tilde{w}$, we compute the free energy for a PM wrapping around an NPL (Fig. 8a). We consider a representative biological membrane with an interfacial tension σ = 0.02 dyn per cm and a bending stiffness $\kappa = 20kT$[24] at room temperature (T = 300 K). By solving the membrane shape equations for a given wrapping degree z (eqn (22)), we obtain the total free energy of the NPL–PM system by summing the elastic free energy of the membrane and the effective attraction induced by the adsorbed biopolymers (eqn (35)). A sufficiently strong NPL–PM attraction ($\tilde{w} > 4$) is required for the NPL to adhere to the lipid membrane and become partially wrapped. In the partially wrapped state, the bio-corona-induced attraction balances the PM's stretching and bending elastic energies.

As the bio-corona-induced NPL–PM attraction strengthens, the partial wrapping degree z (eqn (22)) grows, as evidenced by the shift of the global minimum in total free energy (Fig. 8a). For each z corresponding to the global minimum, we compute the PM elastic free energy (eqn (36)) arising from NPL adsorption (Fig. 8b). Greater wrapping leads to larger elastic deformation of the lipid membrane, enhancing local mechanical stress. Such deformation can destabilize the PM, shortening the lifetime of the biological barrier and potentially triggering cellular or tissue inflammation.[29]

Further strengthening the attraction $\tilde{w}$ shifts the global minimum of the free energy to the fully wrapped state (z = 1), ultimately enabling spontaneous NPL uptake. The phase boundary for spontaneous uptake can be determined by finding the critical $\tilde{w}$ at which the fully and partially wrapped states are equally stable ($\tilde{w} \approx 5.86$). By correlating this critical $\tilde{w}$ with the molecular properties of the adsorbed polymers in the bio-corona, specifically the interaction strengths δ_1 and δ_2 (eqn (20)), we construct a phase diagram describing NPL–PM interactions (Fig. 8c). To facilitate NPL adsorption or uptake, the polymer–PM attraction must be sufficiently strong to overcome the membrane's elastic energy.

The free energy model also permits the estimation of the characteristic time scale of NPL internalization. To do so, we consider the NPLs and lipid membranes to be immersed in water. We thus write the translational (tt) resistance coefficient of the spherical NPL as $\xi_{tt} = 6\pi\eta a^\star$ and the corresponding translational diffusion coefficient as $D_{tt} = kT/\xi_{tt}$, where η = 0.854 mPa s is the dynamic viscosity of water at T = 300 K.[30–32] Using resistance and diffusion coefficients and the free-energy of NPL wrapping (Fig. 8(a)), the mean first-passage time (MFPT) τ for the particle to reach a specific vertical location $h = 2a^\star z$ satisfies the following boundary value problem,[15]

$$-\frac{1}{\xi_{tt}}\frac{\partial \Delta F}{\partial h}\frac{d\tau}{dh} + D_{tt}\frac{d^2\tau}{dh^2} = -1, \quad (38)$$

for which the boundary conditions are: (1) an absorbing boundary at the value of h corresponding to a given wrapping degree z, such that $\tau(h) = 0$; and (2) a reflecting boundary at h = 0, given by $d\tau(0)/dh = 0$.

By solving the MFPT equation, we show that a sufficiently large $\tilde{w}$ is indeed necessary for the NPL uptake. When the fully and partially wrapped states are equally stable ($\tilde{w} \approx 5.86$), the

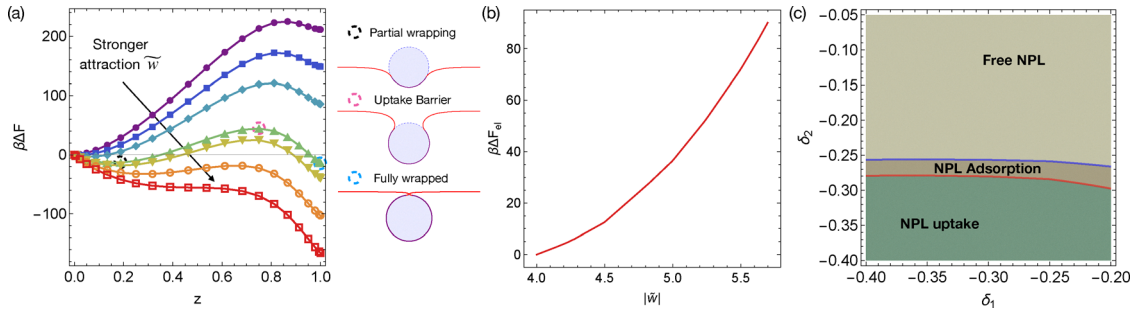

Fig. 8 (a) Free energy of a typical PM wrapping around a model NPL *vs.* bio-corona-induced attraction $\tilde{w}$ ranging from −4 to −7 (eqn (35)). (b) Elastic free energy of the PM induced by NPL adsorption (eqn (36)), corresponding to the global minimum in (a), *vs.* polymer-induced adhesion strength $|\tilde{w}|$. (c) Phase diagram for the model NPL and lipid membrane. Effective NPL radius a^* = 60 nm. Bio-corona consists of polymers of length N = 100 and a Kuhn length b = 1 nm, formed in a solution with $c_0 = 0.1b^{-3}$. PM has an interfacial tension σ = 0.02 dyn per cm and a bending stiffness $\kappa = 20kT$ at room temperature (T = 300 K).

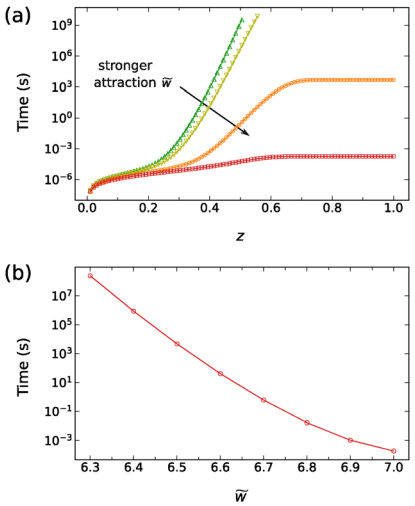

Fig. 9 (a) Mean first-passage-time for an NPL to reach the wrapping degree z. Different colors correspond to the free energy of wrapping in Fig. 8(a) with $\tilde{w}$ ranging from −5.86 to −7. (b) Characteristic time of NPL internalization *vs.* $\tilde{w}$.

uptake barrier (Fig. 8a) prevents internalization as indicated by the diverging MFPT for the system to reach a moderate wrapping degree z. As the attraction $\tilde{w}$ increases, the NPL can be internalized by the cell within hours ($\tilde{w}$ = 6.5) or even in less than one millisecond ($\tilde{w}$ = 7) (orange and red symbols in Fig. 9a, respectively). Nevertheless, by computing $\tau|_{z=1}$, we show that the characteristic time of NPL internalization decreases rapidly with increasing bio-corona-induced NPL–PM attractions (Fig. 9b).

4 Discussion

We expect the theoretical model presented here to be particularly useful for studying interactions between moderately sized NPLs and PM. The spatiotemporal resolution required to characterize the cellular uptake of such NPLs often exceeds the capabilities of conventional simulation techniques, including both atomistic and coarse-grained molecular dynamics.

The input parameters of our model comprise well-documented elastic properties of the PM, such as interfacial tension and bending stiffness, but also include phenomenological interaction parameters used to estimate the NPL–PM adhesion strength w (eqn (21)). These phenomenological parameters (eqn (20)) play a critical role in the adsorption and uptake of NPLs. Sufficient biopolymer–NPL attraction δ_1 is required to form a dense bio-corona around the nanoparticle, while a sufficiently strong biopolymer–PM attraction δ_2 is needed to redistribute adsorbed chains between the two surfaces, enhancing their translation entropy and inducing the NPL–PM attraction.

The parameters δ_1 and δ_2 depend on the molecular structures of biomacromolecules and the compositions of membranes. To quantify their values, we suggest combining atomistic simulations with free energy sampling techniques, such as umbrella sampling and metadynamics.[33] Atomistic simulations could accurately capture the properties of various commodity plastics and lipid membranes, including semicrystallinity[15,34] and elasticity parameters.[35,36] Free energy sampling methods could then be used to compute the binding free energy of a biopolymer on a flat surface, such as a polymer or PM surface. Using metadynamics, Qi and Pfaendtner[37] recently demonstrated how to calculate solid-binding energies of peptides from the binding energies of their residues. We expect that a similar approach could provide reliable estimates of δ_1 and δ_2 for our theoretical model.

Because the lattice SCFT permits the specification of monomer sequences during propagator evolution, the sampled interactions δ_1 and δ_2 from atomistic simulations can be directly incorporated into our model. Our current model "coarse-grains" polymer chains into random walks of Kuhn segments, which are not equivalent to monomeric units such as amino acids. However, our lattice SCFT for flexible polymers can be readily extended to a lattice of semiflexible worm-like chains, where each monomer represents a chemically well-defined moiety.[38] The bending stiffness governing local orientational correlations between adjacent monomers along the semiflexible backbone could then be directly obtained from atomistic simulations. Thus, we expect simulations and free energy calculations based on small systems, such as monomers near

NPL and PM surfaces, could provide quantitative input parameters for the lattice model. Investigating how polymer structure and the surface properties of both the NPL and PM influence adsorption and cellular uptake will be an important direction for future work.

Of course, our simple model here only considered excluded volume interactions and short-ranged interactions for biopolymers. However, proteins are often charged and coordinated by nearby water molecules. To accurately model the adsorption behaviors of biopolymers near NPL and PM surfaces, we will need to incorporate the Poisson–Boltzmann equation into the theoretical framework to account for the electrostatic interactions, which are modulated by added salt in the solution. The polymer physics community has developed self-consistent field theories and scaling arguments to model polyelectrolyte adsorption onto different surfaces,[39] which can serve as the foundation of further refinement of our current approach. Theoretically modeling water-mediated protein–protein interactions, which are governed by the specific amino acid sequence, is challenging. A possible approach to approximate the water-mediated interactions is to perform osmotic pressure simulations[40] of a protein solution. By varying the concentration of proteins in the simulations, one may fit the concentration-dependent osmotic pressure to approximate a two-body effective excluded volume for our model. Testing and validating such an approach are warranted in our future work.

Finally, we would also like to remind the reader that once the NPLs enter the human body, other biological molecules can further modify the surface chemistry of the particles, and in turn, impact their interactions with PMs. For example, the inhaled NPLs and MPLs can be encapsulated by pulmonary surfactants.[41] These bio-coronae formed by lung surfactants can induce attraction between NPLs and PMs and cause lung injury.[42] Thus, we expect the complex molecular environment in biological systems to result in the formation of complex and heterogeneous bio-coronae around NPLs. Quantitatively modeling such adsorption layers around NPLs remains a challenge and is beyond the scope of this paper.

5 Conclusion

By combining the theory of membrane elasticity with polymer physics, we developed a computational framework to predict how the bio-corona influences the adsorption and uptake of moderately sized nanoplastics (NPLs). A lattice-based self-consistent field theory (SCFT) model enables the prediction of bio-corona formation resulting from the adsorption of biopolymers onto an NPL from bulk solution.

Our SCFT model predicts an induced effective attraction between the NPL and PM after re-equilibrating the adsorbed chains between their surfaces. Because bare NPLs composed of commodity plastics such as PE and polypropylene (PP) are repelled by the polar head groups of lipid membranes, this bio-corona-induced attraction is essential for NPLs to adhere to and translocate through the PM.

When the bio-corona induces a sufficiently strong effective attraction, NPLs can adsorb onto PMs and become partially wrapped. The adsorption of NPLs can locally stretch and bend the lipid membrane, potentially generating excess stress and triggering inflammation. Further increasing the effective attraction allows NPLs to be spontaneously internalized by cells, as they become fully wrapped and pinched off. The characteristic time of NPL translocation is strongly affected by the bio-corona-induced NPL–PM interactions and can be estimated using a mean first-passage time analysis (eqn (38)).

Bio-corona-induced attraction depends on polymer properties, including monomer–surface affinity and polymer molecular weight. Although the monomer–NPL and monomer–PM interactions in our current model are phenomenological, we outline how low-cost atomistic simulations and free energy calculations can be used to obtain these input parameters. Indeed, our model here only considers coarse-grained biopolymers as the constituents of bio-coronae. Other molecules in complex biological systems could also adsorb onto NPLs and modify their surface chemistry and interactions with PMs. Still, we expect this work to provide a better understanding of NPL–PM interactions, aiding in the assessment of the potential health impacts of these ubiquitous particles in our environment.

Author contributions

Wenlin Zhang: conceptualization, data curation, formal analysis, funding acquisition, investigation, methodology, project administration, software, resources, supervision, validation, visualization, writing – original draft, and writing – review and editing. Anderson D. S. Duraes: formal analysis, investigation, validation, visualization, writing – review and editing.

Conflicts of interest

There are no conflicts to declare.

Data availability

All numerical data generated using the theoretical tools described in the manuscript are plotted in Fig. 3–9.

Acknowledgements

We acknowledge the startup funding from Dartmouth College that supported this research.

References

1 J. Song, C. Wang and G. Li, *ACS ES&T Water*, 2024, **4**, 2330–2332.
2 N. F. Mendez, V. Sharma, M. Valsecchi, V. Pai, J. K. Lee, L. S. Schadler, A. J. Müller, S. Watson-Sanders, M. Dadmun, G. Kumaraswamy and S. K. Kumar, *Nat. Commun.*, 2025, **16**, 3051.

3 A. D. Vethaak and J. Legler, *Science*, 2021, **371**, 672–674.
4 M. B. Paul, V. Stock, J. Cara-Carmona, E. Lisicki, S. Shopova, V. Fessard, A. Braeuning, H. Sieg and L. Böhmert, *Nanoscale Adv.*, 2020, **2**, 4350–4367.
5 D. M. Mitrano, P. Wick and B. Nowack, *Nat. Nanotechnol.*, 2021, **16**, 491–500.
6 R. Marfella, F. Prattichizzo, C. Sardu, G. Fulgenzi, L. Graciotti, T. Spadoni, N. D'Onofrio, L. Scisciola, R. L. Grotta, C. Frigé, V. Pellegrini, M. Municinò, M. Siniscalchi, F. Spinetti, G. Vigliotti, C. Vecchione, A. Carrizzo, G. Accarino, A. Squillante, G. Spaziano, D. Mirra, R. Esposito, S. Altieri, G. Falco, A. Fenti, S. Galoppo, S. Canzano, F. C. Sasso, G. Matacchione, F. Olivieri, F. Ferraraccio, I. Panarese, P. Paolisso, E. Barbato, C. Lubritto, M. L. Balestrieri, C. Mauro, A. E. Caballero, S. Rajagopalan, A. Ceriello, B. D'Agostino, P. Iovino and G. Paolisso, *N. Engl. J. Med.*, 2024, **390**, 900–910.
7 Y. Wei, H. Chen, Y.-X. Li, K. He, K. Yang and H.-B. Pang, *ACS Nano*, 2022, **16**, 5885–5897.
8 A. Khan and Z. Jia, *iScience*, 2023, **26**, 106061.
9 N. Qian, X. Gao, X. Lang, H. Deng, T. M. Bratu, Q. Chen, P. Stapleton, B. Yan and W. Min, *Proc. Natl. Acad. Sci. U. S. A.*, 2024, **121**, e2300582121.
10 H. Cai, E. G. Xu, F. Du, R. Li, J. Liu and H. Shi, *Chem. Eng. J.*, 2021, **410**, 128208.
11 C. Liu, A. D. S. Duraes, E. L. Jiao and W. Zhang, *MRS Adv.*, 2024, 1–7.
12 O. Hollóczki and S. Gehrke, *ChemPhysChem*, 2020, **21**, 9–12.
13 L. Li, S. Li, Y. Xu, L. Ren, L. Yang, X. Liu, Y. Dai, J. Zhao and T. Yue, *Environ. Sci.: Nano*, 2022, **10**, 440–453.
14 A. Vismara and A. Gautieri, *Biophys. Chem.*, 2024, **308**, 107213.
15 A. D. S. Duraes, E. L. Jiao and W. Zhang, *J. Phys. Chem. B*, 2025, **129**, 3385–3395.
16 H. Garoff, R. Hewson and D.-J. E. Opstelten, *Microbiol. Mol. Biol. Rev.*, 1998, **62**, 1171–1190.
17 M. Zhu, Z. Zhang, T. Zhang, T. Hofmann and W. Chen, *Environ. Sci. Technol.*, 2023, **57**, 331–339.
18 S. Liu, M. Junaid, H. Liao, X. Liu, Y. Wu and J. Wang, *Sci. Total Environ.*, 2022, **836**, 155703.
19 M. D. Lefebvre, M. O. D. L. Cruz and K. R. Shull, *Macromolecules*, 2004, **37**, 1118–1123.
20 N. B. Tito, S. T. Milner and J. E. G. Lipson, *Macromolecules*, 2010, **43**, 10612–10620.
21 N. B. Tito, S. T. Milner and J. E. G. Lipson, *Macromolecules*, 2012, **45**, 7607–7620.
22 W. Zhang, A. Travitz and R. G. Larson, *Macromolecules*, 2019, **52**, 5357–5365.
23 A. N. Semenov, J. Bonet-Avalos, A. Johner and J. F. Joanny, *Macromolecules*, 1996, **29**, 2179–2196.
24 M. Deserno, *Phys. Rev. E*, 2004, **69**, 031903.
25 X. Yi, X. Shi and H. Gao, *Phys. Rev. Lett.*, 2011, **107**, 098101.
26 K. F. Riley, M. P. Hobson and S. J. Bence, *Mathematical Methods for Physics and Engineering*, Cambridge University Press, Cambridge, UK, 3rd edn, 2006, pp. 775–802, 984–1040.
27 U. M. Ascher, R. M. M. Mattheij and R. D. Russell, *Numerical Solution of Boundary Value Problems for Ordinary Differential Equations*, SIAM, Philadelphia, PA, 1995.
28 M. Rubinstein and R. H. Colby, *Polymer Physics*, Oxford University Press, 2003, pp. 309–360.
29 J.-B. Fleury and V. A. Baulin, *Proc. Natl. Acad. Sci. U. S. A.*, 2021, **118**, e2104610118.
30 E. W. Lemmon, I. H. Bell, M. L. Huber and M. O. McLinden, in *NIST Chemistry WebBook, NIST Standard Reference Database Number 69*, ed. P. Linstrom and W. Mallard, National Institute of Standards and Technology, Gaithersburg, MD, 2025.
31 A. D. S. Duraes and J. D. Gezelter, *J. Phys. Chem. B*, 2021, **125**, 11709–11716.
32 A. D. S. Duraes and J. D. Gezelter, *J. Chem. Phys.*, 2023, **159**, 134105.
33 A. Barducci, G. Bussi and M. Parrinello, *Phys. Rev. Lett.*, 2008, **100**, 020603.
34 L. Zou and W. Zhang, *Macromolecules*, 2025, **58**, 3589–3594.
35 K. V. Pinigin, *Membranes*, 2022, **12**, 1149.
36 M. F. Ergüder and M. Deserno, *J. Chem. Phys.*, 2021, **154**, 214103.
37 X. Qi and J. Pfaendtner, *J. Chem. Theory Comput.*, 2024, **20**, 2959–2968.
38 W. Zhang, E. D. Gomez and S. T. Milner, *Macromolecules*, 2016, **49**, 963–971.
39 A. V. Dobrynin and M. Rubinstein, *Prog. Polym. Sci.*, 2005, **30**, 1049–1118.
40 C. Gillespie and S. T. Milner, *Soft Matter*, 2020, **16**, 9816–9821.
41 L. Li, Y. Xu, S. Li, X. Zhang, H. Feng, Y. Dai, J. Zhao and T. Yue, *J. Hazard. Mater.*, 2022, **427**, 127872.
42 X. Xu, R. A. Goros, Z. Dong, X. Meng, G. Li, W. Chen, S. Liu, J. Ma and Y. Y. Zuo, *Environ. Sci. Technol.*, 2023, **57**, 21050–21060.